Light scattering spectra of fast relaxation in silica and $Ca_{0.4}K_{0.6}(NO_3)_{1.4}$ glasses

J. Wiedersich,* N. V. Surovtsev,† V. N. Novikov,† and E. Rössler
Physikalisches Institut, EP II, Universität Bayreuth, Bayreuth 95440, Germany

A. P. Sokolov
Department of Polymer Science, The Akron University, Akron, Ohio 44325-3909
(Received 12 March 2001; published 24 July 2001)

Light-scattering spectra of two glasses, $Ca_{0.4}K_{0.6}(NO_3)_{1.4}$ and silica are measured in the frequency range 1–10 000 GHz, covering temperatures from 19 K to 310 K. The low-frequency wing of the fast-relaxation spectrum is found to show a power-law behavior with an exponent α proportional to temperature at values $\alpha<0.7$. The data are qualitatively and quantitatively compared to different models on relaxations in glasses. It is shown that a model of thermally activated transitions in double-well potentials well describes the fast-relaxation spectra in both materials.

DOI: 10.1103/PhysRevB.64.064207 PACS number(s): 61.43.Fs, 63.20.Pw, 78.35.+c

I. INTRODUCTION

In glass-forming systems one may distinguish fast and slow dynamics. Usually, slow dynamics refers to the primary α-process that is a characteristic feature of supercooled liquids. Typically this relaxation process appears below the GHz band and exhibits a strong temperature dependence. In contrast, fast dynamics are observed in the GHz regime and show a weak temperature dependence. They persist in the glass, i.e., below the glass transition temperature T_g. Over the past decade, interest on fast dynamics has been strongly stimulated by predictions of the mode-coupling theory (MCT) of the glass transition.[1] Another origin of fast dynamics may be expected due to the dynamics in asymmetric double-well potentials (ADWP), which play an important role for the understanding of the low-temperature anomalies of glasses.

Experimentally, fast dynamics show up as a broad quasielastic contribution in neutron[2–6] and light-scattering spectra.[7–22] Fast relaxation processes were recently also observed in dielectric measurements.[23] Due to the much lower amplitudes, relaxations in glasses, i.e., below T_g, are usually studied by different techniques as compared to those employed at higher temperatures. For example, they are probed as a damping of sound waves as seen in experiments on ultrasonic attenuation or internal friction.[24–36] Some investigations of fast relaxations in glasses used neutron or Raman spectroscopy. However, respective spectrometers have a low-frequency limit around 50 GHz. In these spectra relaxation processes are reflected by a quasielastic component that dominates the spectra at frequencies below 300–500 GHz and does not show a harmonic temperature dependence. Developments of tandem Fabry-Perot interferometers (TFPI) opened the possibility to measure light-scattering spectra in a broad frequency range down to ~1 GHz. This technique has been actively applied over the past years for the investigation of glass-forming liquids above and around the glass transition temperature T_g (see, e.g., Ref. 6,12,13,17,18). To the best of our knowledge, only a few investigations of fast relaxational spectra in glasses covering a broad frequency and temperature range have been reported so far.[18,22,21] Employing TFPI at temperatures below T_g, special care has to be taken in order to be able to sample signals of low amplitudes.

The nature of relaxations in glasses ($T<T_g$) is still not well understood. At temperatures deep in the glassy state (at temperatures above ~10 K), thermally activated transitions in ADWP's are assumed to give the main contribution to the fast-relaxation spectrum.[18,29,37,38,40] Assuming that ADWP's determine the dynamics, many authors have successfully applied this approach for the description of internal friction or light-scattering data above ~10 K.[18,25,27,29,30,34–38,40] Another phenomenological model of the fast dynamics in glasses is the soft-potential model (SPM).[41] This model describes tunneling systems, relaxations in ADWP's and soft vibrations, i.e., the so-called boson peak. Since at present the SPM is one of the most successful approaches for the description of the dynamics in the glassy state and since it makes detailed predictions we pay much attention to the analysis of our data within the frame of this model. Recently, it was shown that anharmonicity of vibrations may also contribute to the fast relaxation and this contribution may be dominant at high enough temperatures.[42] We discuss the contribution of this relaxation process for the systems investigated here. Briefly, we also consider some other models.

The main goal of the present paper is to report in detail our TFPI measurements of fast-relaxation spectra at temperatures well below T_g ($32\,K<T<310\,K$). First reports concerning different aspects were given in Refs. 18,21,22. We measured the depolarized light scattering spectra of two paradigmatic glasses, $Ca_{0.4}K_{0.6}(NO_3)_{1.4}$ (CKN) and silica, over a broad frequency range from 1 GHz to 10 THz. Special attention was given to the suppression of intensity from higher orders of the TFPI. In particular, we apply additional interference filters and we demonstrate their effect on the measured spectra. As was shown first by our group and shortly after by Gapiński *et al.*[19] and Barshilia *et al.*,[20] measurements without such filters lead to severe distortions of the low-intensity spectra, in particular at low temperatures, where the signal from the relaxational contribution is weak. In comparison to our previous publication[18] the data on CKN are extended to lower frequencies. We perform an analysis of

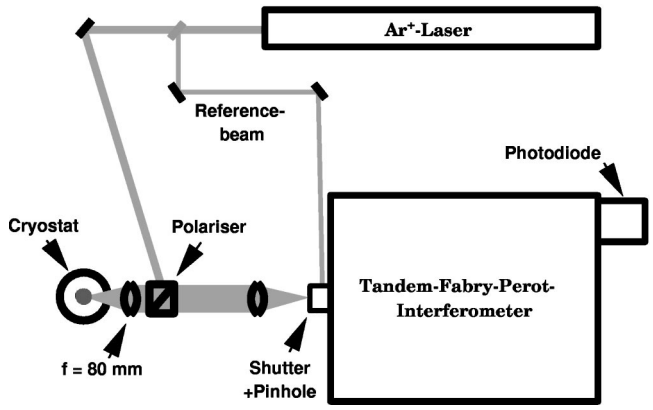

FIG. 1. Experimental setup of the total-backscattering experiment. The Glan-laser polarizer is used as a beam splitter in order to select the depolarized component of the scattered light.

the data within the frame of the models discussed above. In particular, we show that the light-scattering data, covering a broad temperature and frequency range, allow to extract the distribution of barrier heights $g(V)$ of the ADWP's discussed within the model of Gilroy and Phillips.[29] The results on $g(V)$ are compared with those obtained from internal friction measurements.[25,27,35,36] Up to now, the latter model was only tested by studying the temperature dependence at a few single frequencies. Our TFPI measurements of the fast-relaxation spectra provide a more stringent test, since we can validate the predictions of the model on both the temperature and frequency dependence of the relaxations.

The paper is organized in the following way. In Sec. II the experiment and samples are described in details. Section III shows our experimental results, which are discussed in the frame of different models on relaxations in glasses in Sec. IV. Section V presents the Conclusion.

II. EXPERIMENT

Two glasses, CKN and silica (Heralux, Heraeus, 130 ppm OH^- groups and Suprasil 300, Heraeus, <1 ppm OH^- groups) are studied. The CKN sample was described in a previous publication.[43] For the CKN and Heralux samples we used a near-to-backscattering geometry (see below), while the Suprasil experiments were carried out in a total-backscattering geometry (where the scattering volume is largest) in order to maximize the collection of scattered light in view of the low intensities.

Silica (Suprasil 300). Depolarized inelastic light-scattering spectra of the sample of Suprasil 300 were obtained using an Ar^+, laser (514.5 nm, 400 mW) and a six-pass Sandercock TFPI.[45] The sample was mounted in a dynamic Helium cryostat. The Suprasil windows of the cryostat are antireflection coated, and the cold windows are mounted tensionless in order to avoid tension-induced birefringence. Since the signal levels available from the scattering of silica are much lower than for other glasses studied so far,[18,21] the optical scheme, that is shown in Fig. 1, was improved and optimized for alignment on low intensities.[46] We use a 180° back-scattering geometry with a selection of depolarized scattering. Here the laser beam enters a Glan-Taylor polarizer (extinction 10^{-6}) as the extraordinary beam. The polarized component of the light is reflected and focused on the sample. The scattered light is collected by the same lens and passes through the same Glan-Taylor prism, transmitting the depolarized component. The scattered light is collected within an angle of about 4°. Special care was taken to avoid contributions to the signal from the windows of the cryostat and the polarizer. This background has been carefully measured for all temperatures and free spectral ranges by recording spectra with and without sample. At all settings we find a background of about 3% of the signal, relating it to a contribution from the cold windows, which are close to the focus of our lens, basically at the same temperature as the sample, and of the same material as the sample. Nevertheless, we carefully eliminated its contribution by subtracting the signal from accumulations without sample from all of our spectra.

We recorded spectra with the free spectral ranges (FSR's) of 1000 GHz and 150 GHz over two spectral ranges on either side of the elastic line. The experimentally determined finesse of the spectrometer is better than 120 and typically about 140. In order to suppress higher transmission orders of the TFPI [multiples of 20 FSR's could give contributions to the signal for a Sandercock tandem FPI (see below)[18–20,45]], we use a prism in combination with either of two interference filters of a width of 11 300 and 1150 GHz [full width at half maximum (FWHM)]. The contrast of the spectrometer (defined here as the ratio of the maximum transmission for the zero order and the highest value of elastic signal in the range $0.07\ \mathrm{FSR} < \nu < 0.93\ \mathrm{FSR}$) was determined to be better than 10^9 at all frequencies.

To further validate the absence of possible contributions from the instrumental tail of the elastic line or from higher transmission orders of the TFPI, we measured spectra for both FSR's at a low temperature, $T = 6$ K. At this temperature the anti-Stokes part of the spectrum should be almost zero because either the Bose factor or the signal itself are very low for this temperature. Indeed, the anti-Stokes part of the spectrum at this temperature shows no deviations from the dark count level of 2.47 counts/s of our detector, demonstrating the absence of contributions of higher orders or from the elastic line. Special care should be taken in order validate the absence of any contributions from higher orders in the case of the smaller FSR, because the signal is much higher at frequencies of multiples of 20 of this FSR than in the range of interest: the signal increases with increasing frequency, especially at low temperatures, where the relaxational contribution is small (cf. Figs. 2 and 3). For our 6 K-spectrum in this region the sum of the signal and possible higher order contributions is less than 0.3 counts/s, i.e., it is absent within the precision of our experiment. Since the vibrational part, that could lead to any parasitic contributions, rises much slower with temperature than the signal from relaxations, it is clear that signals from higher transmission orders do not disturb our spectra.

CKN and silica (Heralux). We used a conventional near-backscattering setup (at a scattering angle of some 172°), employing the same interferometer and laser. The typical

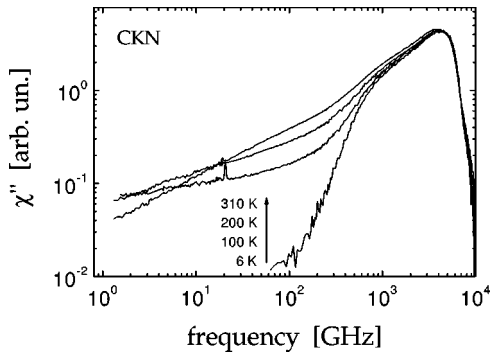

FIG. 2. Light-scattering susceptibility spectra of CKN at different temperatures. The Raman data for $\nu \geqslant 150$ GHz are taken from Ref. 15.

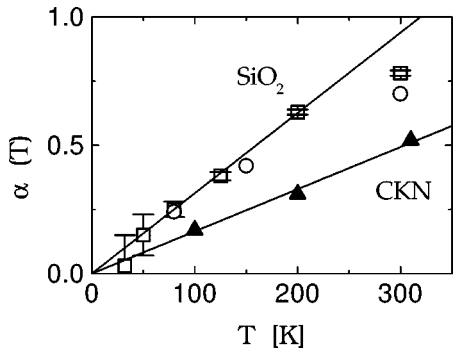

FIG. 4. Temperature dependence of the exponent α obtained from the spectra for CKN (▲) and silica (Heralux: ○, Suprasil 300: □).

power of the focused beam was 200 mW. The geometry of this setup excludes any contributions to the spectrum from cryostat windows and (in the case of CKN) the cuvette that contains the sample. The data on Heralux served as a double cross-check to further validate the results on Suprasil 300. The thus recorded spectra agree with the results reported for Suprasil within our accuracy (cf. Fig. 4). A polarizer (Glan laser prism, extinction coefficient $>10^6$) and an analyzer (Glan-Thompson prism, extinction coefficient $>10^5$) were used for the incident and scattered light, respectively. The crossed orientation of the polarizer and analyzer selects the depolarized light scattering geometry (VH geometry). In order to cover a broad frequency range, for each temperature spectra of CKN were obtained measuring with different mirror spacings, corresponding to FSR 300, 37.5, and 10 GHz. In the case of Heralux we obtained spectra with the FSRs 50 GHz and 200 GHz. For every mirror spacing, spectra were measured in a double-scan regime, collecting spectra up to ± 2 FSR. The contrast of the apparatus was determined by using elastically scattered light from a metal bar. The experimentally measured contrast for the lowest FSR = 10 GHz was better than 10^{10} at all frequencies larger than 1 GHz, allowing us to suppress the elastic line contribution down to 0.07 FSR. The suppression of the elastic line was further checked in the case of FSR=10 GHz by comparing the measured spectral shape with another one using FSR =9 GHz, like it is usually done in the Raman technique (see, e.g., Ref. 44). At higher FSRs the contrast was better than 10^9. The typical ratio of overlapping frequencies between adjacent spectra was about 3.

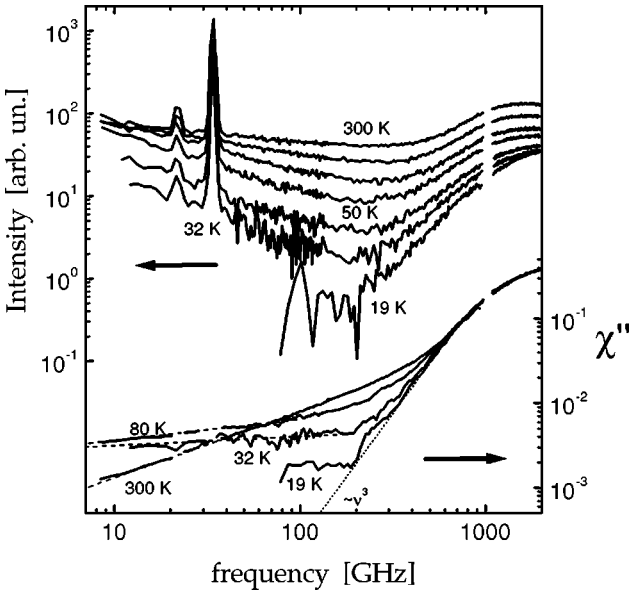

FIG. 3. Light-scattering spectra of silica glass (Suprasil 300): intensity spectra for the temperatures 300 K, 200 K, 125 K, 80 K, 50 K, 32 K, and 19 K (from top to bottom, left scale: for the FSR 1000 GHz the left scale approximately reflects the count rate in Hz, for the lower FSR it is lower by about a factor of 5) and susceptibility spectra $\chi''(\nu)$ for the temperatures 300 K, 80 K, 32 K, and 19 K (below, right scale, smoothing over five data points). The data are scaled to match at high frequencies, where it is known that the temperature dependence of the susceptiblity is small in our temperature range (Ref. 54). The dashed lines show a power-law fit to the low-frequency wing of the data. The steepest part of the 19-K spectrum can be fitted by a ν^3 law (dotted line).

As already noted in Ref. 18 and further shown in Refs. 19 and 20 even in a tandem configuration of two FPIs, higher orders (here multiples of 20) may give a contribution to the signal and distort the shape of the spectra (see also Ref. 45). Therefore appropriate interference filters and a prism were used to suppress these contributions. Measuring the calibrated spectrum of a halogen lamp with and without the filters, we observed that in the case of a flat spectrum higher-order contributions in absence of the interference filter add about a factor of 2.3 of the actual signal for a FSR of 10 GHz (see also Ref. 46). The resulting distortion of the spectra is shown in Figure 5, where we compare our results for CKN at room temperature obtained with and without the interference filters. We used an interference filter with a width (FWHM) of 1150 GHz for FSRs of 37.5 GHz and higher, and one with a FWHM of 185 GHz for the lower FSR's. In order to arrive at the final broad-band spectra, the spectra of smaller FSR's were scaled in order to mach the spectra obtained at higher frequencies (for the monochromator data, there are no higher-order contributions). Therefore, the fact, that the curve recorded without filters lies below the one recorded employing the filters, reflects the *different spectral shapes* of

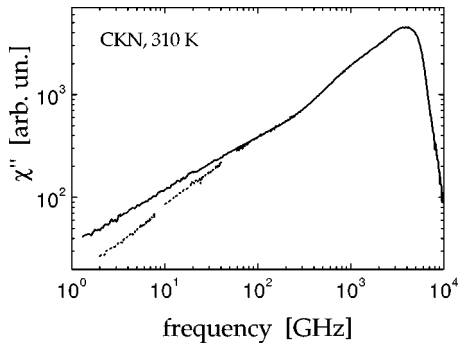

FIG. 5. Light-scattering susceptibility spectra of CKN, recorded with (solid line) and without (dotted line) the use of appropriate interference filters as discussed in the text. The amplitudes of the spectra are chosen in a way to provide a matching at high frequencies. Without these filters a downward curvature of the spectra (a *knee*) is observed; on applying the additional filters we observe a power-law behavior for the low-frequency wing of our spectra.

the spectra, not the different absolute amplitudes of the recorded signals.

On applying the interference filter, one has to make sure that the resulting spectra are not distorted by the transmission and sensitivity of the tandem FPI/prism/filter/detector combination. Therefore the transmission of the spectrometer was determined by recording spectra of a calibrated halogen lamp before and after the accumulation of each spectrum. The comparison of these spectra also ensured that the transmission function did not change over the course of the experiment. This could be the case, if a mode hop of the laser or a significant change of the temperature within the spectrometer occurred. In the rare events, when this was the case, the experiment was repeated. The measured spectra were corrected by the dark count level of the detector and normalized to the spectra of the calibrated lamp. After the normalization, the Stokes and anti-Stokes sides of the spectra were compared, taking into account the Boltzmann factor for the different temperatures and frequencies. It turns out that the Stokes and anti-Stokes sides of all spectra agree within the signal-to-noise ratio, confirming the quality of our data. In the case of low temperatures and high frequencies, where the Boltzmann factor significantly differs from 1, this also confirms the temperature of the illuminated volume of the sample.

To further validate the quality of the spectra, we additionally performed measurements with FSR of 150 and 20 GHz at some temperatures in order to check the overlap of different spectra. On using the interference filters, within the overlapping regions the spectral shapes obtained from different free spectral ranges were the same with a typical precision of about 1%, i.e., within our signal-to-noise ratio. For temperatures where the additional FSR were used, the overlap between adjacent FSR's was a factor of 8. This result demonstrates the absence of parasite contributions from higher-transmission orders.

Looking at the two data sets in Fig. 5 it is obvious that a kind of *knee* appears when no interference filters are applied. The origin of this kind of spectral distortion was discussed in Refs. 18,22,19,20,46. The knee was erroneously taken as a signature of MCT prediction below the critical temperature T_c (cf. also below).

In the case of CKN, the experiments were performed at 10° and 170° scattering angles for FSR 37.5 GHz and higher. For the lower FSR and for silica (Heralux), spectra were only recorded for the backscattering geometry. In order to obtain the combined spectra we used the 10° experiment, where the Brillouin lines that correspond to backscattering are suppressed much better; however, even in this case they disturb the spectra due to a contribution from the incident beam reflected from the surfaces of the sample.

III. SPECTRAL SHAPE OF THE FAST RELAXATION

A. Light-scattering spectra

The measured spectra, in the case of CKN combined with previously reported Raman data,[43] are presented in Figs. 2 and 3 as the dynamic susceptibility

$$\chi''(\nu)=\frac{I(\nu)}{n(\nu)+1}, \tag{1}$$

where $n(\nu)$ is the Bose factor. The spectra of both samples exhibit a power-law tail at low frequencies ($1\,\mathrm{GHz}<\nu<100\,\mathrm{GHz}$). At higher frequencies the spectra exhibit the boson peak and the microscopic peak. In the case of CKN the shoulder at 200–500 GHz corresponds to the boson peak. The small but sharp peak at 10–15 GHz is a leakage of the longitudinal Brillouin line. For silica, the leakage of the Brillouin lines leads to the peaks at 21 and 33 GHz. The gaps in the spectra around 1000 GHz in the case of silica are due to the so-called ''ghost lines'' of the tandem FPI, which have been removed from the data.

In the case of CKN the tandem FPI data have been scaled to the high-frequency Raman data. In the case of silica, where we do not have the Raman data, the susceptibilities of the data were scaled to match at high frequencies. It is known from the literature that the amplitude of the boson peak in silica decreases by about 30% in the range from 50 K to 1100 K (cf. Ref. 54). In our temperature range, however, this change is negligible.[54] The factors for the scaling were always less than 25%, i.e., the absolute count rate was reproducible within that range. This value demonstrates the high quality of our setup: due to the low signal levels we were not able to realign on the sample during the Suprasil experiment, which took a few weeks.

At the lowest temperature the quasielastic scattering is negligible and the spectrum represents essentially vibrational contributions, $\chi''_v(\nu)$. It is obvious that at higher temperatures in the region of the power-law behavior $1\leqslant\nu\leqslant100$ GHz, the vibrational contribution can be neglected and the fast-relaxation contribution $\chi''_r(\nu)$ dominates the spectra. Contrary to the vibrational contribution, the relaxational one strongly depends on temperature. The exponent of the low-frequency power-law behavior (the apparent slope in a log-log plot) is less than 1 and depends on temperature and sample. We note that no knee, i.e., a transition from a power law with an exponent α less than unity to a white noise spectrum ($\alpha=1$) at lower frequencies, is observed (cf.

Figs. 2 and 3). It should be emphasized that instead of a transition to a white-noise spectrum the exponent α becomes smaller with decreasing temperature both for CKN and silica. Within MCT this knee is predicted for temperatures below the critical temperature T_c, although the apparent absence of the knee may be explained in the presence of additional relaxation processes (hopping) that are believed to dominate the dynamics below T_c. Our result disagrees with the data of Ref. 11, where indications of this knee were found for CKN around T_g. We attribute this difference to the suppression of higher orders of the TFPI in our experiments due to the use of interference filters, which the authors of Ref. 11 did not use (cf. Sec. II). The absence of that knee for some polymeric glasses and CKN was observed earlier[18] and very recently in Refs. 19 and 20 where the knee in CKN spectra was not confirmed at temperatures above T_g. Thus we conclude that on measuring broad-band TFPI spectra, additional interference filters have to be applied in order to avoid artifacts. The testing of MCT below the critical temperature T_c by light scattering remains a future task.

For CKN the spectral shapes obtained at the two different scattering angles of 10° and 170° were the same with a precision of better than 1% (except for the range around the Brillouin lines). We conclude that the spatial extent of the structural rearrangements responsible for the fast relaxations is much less than the wavelength of the light; this would explain the same results for the 10°- and 170°-scattering experiments.

B. Separation of the fast-relaxation spectrum

The measured light scattering spectra contain both relaxational and vibrational contributions. In order to obtain the spectrum of fast relaxations, the vibrational contribution should be accounted for at each temperature. In the region of the low-frequency tail (1–100 GHz) the relaxational contribution dominates and vibrational contributions can be ignored. On the other hand, it is obvious from Figs. 2 and 3 that the vibrational contribution is dominant at higher frequencies. To get a better idea of the spectral shape of the relaxations, we assume that the relaxational spectrum can be obtained by a subtraction of the vibrational contribution from the experimental spectrum. This assumption is justified if the relaxation is weak in the sense that the broadening of the vibrational modes due to relaxation is much smaller than the vibrational frequency.[14] This condition is normally satisfied well below the glass transition temperature (see, e.g., Refs. 14,15). We note that such a subtraction does not contradict the damped oscillator model of the fast relaxation, where the latter can be observed only via the relaxational part of the vibrational susceptibility[14] (this point will be considered in more detail below). The vibrational spectrum can be obtained by measurements at low enough temperatures where the relaxational contribution becomes negligibly small. In a rough approximation this low-frequency vibrational spectrum can be used for the subtraction also at higher temperatures; however, to improve the accuracy one needs to take into account the shift and the change of the amplitude of the vibrational spectrum with changing temperature. Therefore we also consider the evolution of the vibrational spectrum with temperature.

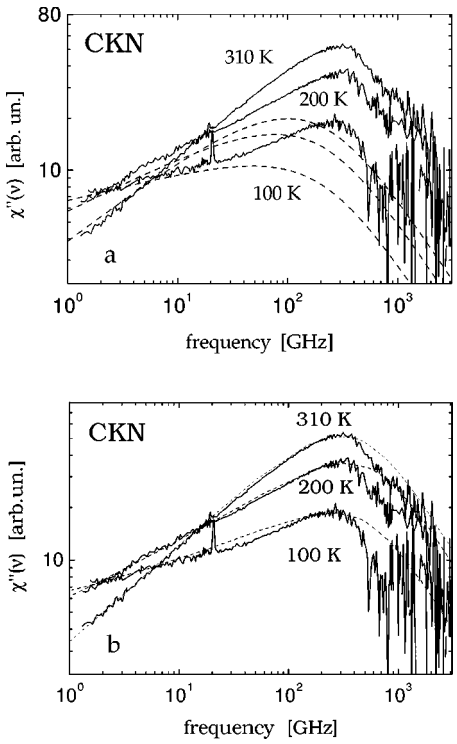

FIG. 6. Fast-relaxation susceptibility spectra of CKN obtained after subtraction of the vibrational contribution (solid lines). (a) Fit of the experimental relaxation spectra, $\chi''_r(\nu)$, for CKN by the ADWP model, Eq. (6), with an exponential distribution of barrier heights, Eq. (9) with $V_0 = 570$ K, (dashed lines). (b) Fit by the generalized soft-potential model, Eq. (34) (dashed lines). The parameters of Eq. (34) are: $b = 0.45$, $V_0 = 600$, 910, and 1250 K for $T = 310$, 200, and 100 K, respectively.

For CKN we took the Raman spectrum at $T = 6$ K as the low-temperature vibrational contribution. To obtain the vibrational spectrum at frequencies 1–100 GHz, we extrapolate the low-frequency wing of the vibrational spectrum by a power law $\chi''_v(\nu) \propto \nu^3$. According to the Shuker-Gammon expression[47] $\chi''_v(\nu) \propto C(\nu) g(\nu)/\nu$ this choice corresponds to a Debye-like spectrum of the vibrations,[48] i.e., $g(\nu) \propto \nu^2$ and $C(\nu) \propto \nu^2$, where $g(\nu)$ is the vibrational density of states and $C(\nu)$ is the light-to-vibration coupling constant. In order to take into account the temperature dependence of the vibrational spectrum due to quasiharmonic softening of the lattice we shift the whole vibrational spectrum according to the shift of the microscopic mode at ~3000 GHz. However, it is observed that the shift of the subtracted vibrational spectrum does not change the low-frequency wing and the whole qualitative picture of the relaxation spectrum. As already mentioned, this is expected, because the vibrational contribution is negligible at low frequencies in these glasses, and the shift of the vibration band in our conditions is small. In Fig. 6 the relaxational spectra of CKN obtained by subtracting the shifted vibrational band are shown.

In the case of silica, basically the same procedure was used to obtain the relaxational contribution as it is displayed in Fig. 7. Here we have no high-frequency data in order to

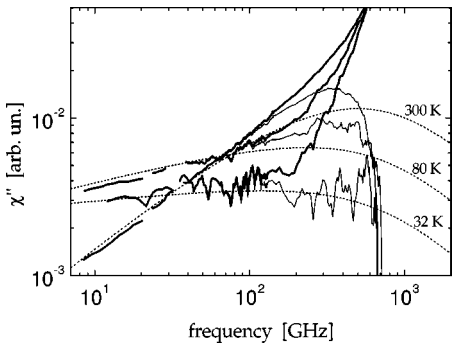

FIG. 7. Comparison of numerical evaluations of Eq. (6) with an exponential $g(V)$ (dotted lines) with the light-scattering data for Suprasil 300 [thick lines: measured susceptibility $\chi''(\nu)$, thin lines: relaxational contribution $\chi''_r(\nu)$].

consider the shift of the Boson peak. However, it is known that this shift is very small in our temperature range (cf. e.g., Ref. 54).

C. Properties of the fast-relaxation spectra

The relaxation spectra (Figs. 6, and 7) show several characteristic features.

(i) The position of the maximum, ν_0, i.e., the respective relaxation time τ_0 is essentially temperature independent; $\nu_0=(2\pi\tau_0)^{-1}=275$ GHz (400 GHz), so $\tau_0\approx 0.6$ ps (0.4 ps) for CKN (and silica).

(ii) The high-frequency part shows approximately Debye behavior not too far from the maximum (dashed line) and a much faster decay at higher frequencies.

(iii) The amplitude of the maximum of the relaxation spectra increases significantly with temperature.

(iv) The low-frequency wing is described by a power law

$$\chi''_r(\nu)\propto\nu^{\alpha},\quad 2\pi\nu\tau_0\ll 1, \tag{2}$$

with a temperature-dependent exponent $\alpha<1$. This exponent α is independent of the substraction procedure employed and can actually be obtained directly from the light-scattering spectrum without subtraction of the vibrational contribution since the latter is negligible at low frequencies. Both in CKN and SiO_2 the exponent α increases roughly proportional to temperature (cf. Fig. 4),

$$\alpha=bT \tag{3}$$

where $b^{-1}=610$ K and 319 K in CKN and silica, respectively. In the latter case deviations of the temperature dependence of α from the linear law (3) are evident at room temperature where $\alpha=0.7$; on very general grounds, one expects that at higher temperatures α will not exceed 1, i.e., a white-noise exponent (cf. below). Indeed at higher temperatures up to T_g it is found that the exponent remains constant at 1 (Refs. 46,49).

Let us note that according to Ref. 18 also for other systems like polymers a power-law behavior is observed, although the temperature dependence of the exponent α in polymers is not so simple and universal. In polystyrene (PS) α increases with temperature as a linear function (but not proportionally to T) up to room temperature where it reaches a level of 0.6. In the case of polycarbonate (PC) and anorganic B_2O_3 glass α does not increase with temperature and is approximately a constant equal to 0.3 in PC Ref. 18 and 0.6 in B_2O_3.[21] On the other hand, the temperature dependence of α shows very similar behavior in CKN and silica and therefore a common discussion is justified.

Two reasons may be responsible for an increase in the amplitude of the fast relaxation spectrum with temperature. First, an increase in the number of relaxing units may lead to an increase in the relaxation amplitude. Second, even if the number of the relaxators is constant, the amplitude of the fast relaxation at high frequencies, near the maximum, may increase on the expense of the low-frequency part of the spectrum. This is nothing else than to assume a distribution of correlation times. The second mechanism is in agreement with the observed increase of α with temperature, compare, below. In order to compare the relaxational contributions of CKN and silica it is convenient to consider the ratio of the integral over the spectral density of relaxations,

$$S_r\equiv\int_0^{\infty}\chi''_r(\nu)\frac{d\nu}{\nu}, \tag{4}$$

to the respective integral over the vibration spectrum, $S_v=\int_0^{\infty}[\chi''_v(\nu)/\nu]d\nu$. The parameter

$$\delta_0^2=\frac{S_r}{S_r+S_v} \tag{5}$$

characterizes the integral strength of the fast relaxation in comparison with that of vibrations (the parameter δ_0^2 was used in some previous publications,[7,10,14,15,40] so we use the same symbol). The integral (4) for CKN can be found directly using the spectra of Fig. 6. At low frequencies we extrapolate the spectrum by the power law with the exponent α. The calculation shows that in CKN δ_0^2 increases only by 20% from $T=100$ K up to room temperature with an average value $\delta_0^2=0.23$ in this temperature interval. In silica a comparison of S_r with the integral over the Raman spectrum taken from literature[40] gives $\delta_0^2\sim 5\%$ at room temperature, in agreement with the result of Ref. 40; within the accuracy of the experiments we find no temperature dependence of δ_0^2. An increase of δ_0^2 is due to an increase of S_r; the integral over vibrations does not change within the accuracy of the experiment. We note that the magnitude of the parameter δ_0^2 in these two glass formers correlates with the degree of fragility: it is higher in the fragile CKN and lower in the strong silica. This is in agreement with the observation[15,50] that δ_0^2 taken at some reference temperature, e.g., T_g, may be taken as a measure of the degree of fragility.

IV. MODELS OF FAST RELAXATION

Now we turn to the analysis of the relaxation spectra compiled in Figs. 6 and 7 within the frame of existing models.

A. Mode-coupling theory

As discussed, a power-law behavior of χ_r'' and a transition to a white-noise spectrum at lower frequencies (the so-called *knee*) are asymptotic predictions of the idealized version of MCT.[1] These predictions are expected to hold for the temperature range around the critical temperature $T_c > T_g$. In particular, the slope of the low-frequency tail of the fast-relaxation spectrum is expected to be less than 0.4. Schematic versions of MCT with inclusion of an additional hopping term can be applied to describe the spectra of the fast relaxation below T_c and hopping may obscure the presence of the *knee*. Up to now there are no quantitative predictions, e.g., regarding the position of the knee or the slope α for disordered materials below the glass transition point.

B. Relaxation in asymmetric double-well potentials

1. Quasielastic spectrum

In 1955 Anderson and Bömmel attributed relaxations in silica glass to thermally activated processes with a broad distribution of barrier heights.[25] Theodorakopolous and Jäckle ascribe the quasielastic scattering of glasses to the relaxation in double-well potentials (DWP) and have shown its relation to the acoustic attenuation.[37] The model was generalized by Gilroy and Phillips[29] and Jäckle[38] to take into account the *asymmetry* of the DWP's that is expected for disordered solids. The ADWPs responsible for the thermally activated transitions are assumed to be the same that at lower temperatures ($T < 1$ K) relax via tunneling and are responsible for the low-temperature anomalies of glasses.[39]

Within this model the Raman susceptibility (1) is obtained by integrating over the distributions of barrier heights $g(V)$ and asymmetry parameters $f(\Delta)$ of the ADWP's (Ref. 29)

$$\chi_r''(\nu) = \frac{A}{T}\int_0^\infty \int_0^\infty \frac{2\pi\nu\tau}{1+(2\pi\nu\tau)^2}\,\mathrm{sech}^2\left(\frac{\Delta}{2T}\right) f(\Delta) g(V)\, d\Delta\, dV, \tag{6}$$

where A is a constant. If the thermal energy is high enough with respect to the asymmetry parameter Δ, i.e., $\Delta < 2T$, and the distribution function of Δ is flat, $f(\Delta) = f_0 = \text{const}$, Eq. (6) reduces to[37,29,34,36]:

$$\chi_r''(\nu) \approx 2A f_0 \int_0^\infty \frac{2\pi\nu\tau}{1+(2\pi\nu\tau)^2} g(V)\, dV. \tag{7}$$

Here $g(V)$ is the distribution of barrier heights V, and the temperature dependence of the relaxation time is determined by a thermally activated process,

$$\tau = \tau_0 \exp(V/T). \tag{8}$$

where τ_0 is determined by the attempt frequency. Assuming, for example, an exponential distribution of barrier heights,

$$g(V) = V_0^{-1} \exp(-V/V_0), \tag{9}$$

Eq. (6) gives

$$\chi_r''(\nu) = \pi f_0 \alpha A (\nu\tau_0)^\alpha \int_{2\pi\nu\tau_0}^\infty \frac{x^{-\alpha} dx}{(1+x^2)^{1/2}[1+(1+x^2)^{1/2}]}, \tag{10}$$

where $x = 2\pi\nu\tau$ and the exponent α is proportional to temperature,

$$\alpha = T/V_0, \quad T < V_0. \tag{11}$$

For $2\pi\nu \ll \tau_0^{-1}$ Eq. (10) predicts a power-law susceptibility spectrum,

$$\chi_r''(\nu) \approx \pi f_0 \alpha A (2\pi\nu\tau_0)^\alpha, \quad 2\pi\nu \ll \tau_0{}^{-1}. \tag{12}$$

Since τ_0 provides a cutoff of the correlation-time distribution corresponding to Eq. (10), the latter predicts a Debye behavior at high frequencies,

$$\chi_r''(\nu) \approx \frac{\pi f_0 \alpha A}{\alpha+1} (2\pi\nu\tau_0)^{-1}, \quad 2\pi\nu \gg \tau_0^{-1}. \tag{13}$$

The exponent α for CKN and silica in Fig. 4 show the expected proportionality to temperature (11). Some deviations from the proportionality appear in silica at room temperature. As discussed, these deviations are not surprising when α is close to 1 since the exponent α cannot be higher than 1 in the frame of the (A)DWP model.

At low frequencies, the experimental data of CKN and silica are in excellent agreement with the predictions of the ADWP model of a low-frequency power law of the susceptibility, Eqs. (12) and (13). As it will be shown in the following section, the temperature dependence of the amplitude of the low-frequency wing of the spectra is in excellent agreement with the ADWP model as well.

2. Extraction of the barrier distribution

Equation (7) can be further simplified assuming a broad distribution $g(V)$ as is expected for glasses, so that in comparison with $g(V)$ the function $2\pi\nu\tau/[1+(2\pi\nu\tau)^2]$ is a relatively sharp peak at $2\pi\nu\tau \sim 1$. A convolution of a narrow and a broad function gives to good approximation the broad function. As a result, the susceptibility spectrum $\chi_r''(\nu)$ directly reflects the distribution of correlation times, and thus the distribution $g(V)$[36,51]:

$$\chi_r''(\nu) \propto T\, g(V(\nu)), \quad \text{where} \quad V(\nu) = T \ln(1/2\pi\nu\tau_0). \tag{14}$$

Assuming that $g(V)$ is essentially temperature independent and that thermally activated transitions in ADWP's determine the light-scattering spectra up to room temperature and 200 K for CKN and silica, respectively, $g(V)$ can directly be extracted from each susceptibility spectrum in Figs. 6 and 7 (or indeed Figs. 2 and 3) by rescaling the axes with T. Explicitly, we multiply the $\ln(\nu)$-axis by T and divide $\chi_r''(\nu)$ by T. Then a master curve for $g(V)$ should result from $\chi_r''(\nu)$ for all temperatures. The only free parameter is $2\pi\nu_0 = \tau_0^{-1}$. We use $\nu_0 = 150$ GHz for CKN and 800 GHz for silica, respectively, at all temperatures. These values provide the best agreement of the data; for CKN this value of ν_0 is

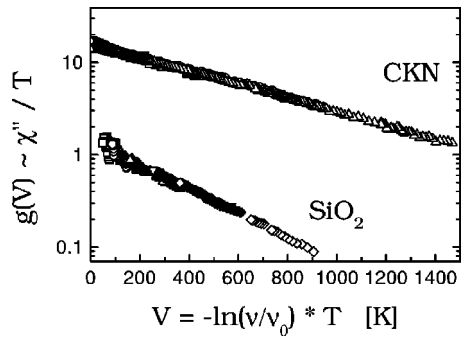

FIG. 8. Distribution of barrier heights $g(V)$ (obtained from the light-scattering spectra of Fig. 2. Plotted are the data sets of 100 K (□), 200 K (○), and 310 K (△) (CKN); 32 K (□), 50 K (○), 80 K (△), 125 K (▽), 200 K (◇) (silica).

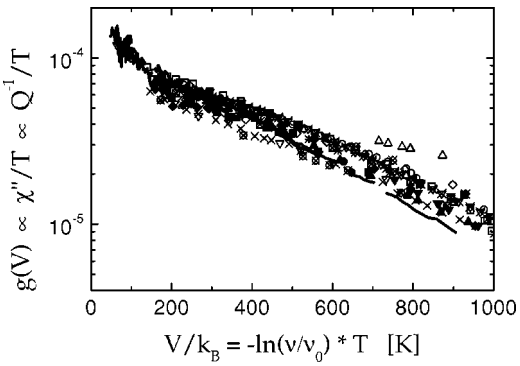

FIG. 9. Distribution of barrier heights $g(V)$ for silica obtained from light scattering (solid lines: $T=32$, 50, 80, 125, 200 K) and internal friction (symbols). symbols: solid squares, 35 GHz (Ref. 28), solid circles, 930 MHz (Ref. 26), solid up triangles, 748 MHz (Ref. 26), solid down triangles, 507 MHz (Ref. 26), solid diamonds, 330 MHz (Ref. 26), open squares, 43 MHz (Ref. 31), open circles, 20 MHz (Ref. 25), open up triangles, 10 MHz (Ref. 24), crosses, 660 kHz (Ref. 29), open down triangles, 201 kHz (Ref. 24), open diamonds, 180 kHz (Ref. 35), crossed squares, 90 kHz (Ref. 33), crossed circles, 66 kHz (Ref. 24), crossed down triangles, 11.4 kHz (Ref. 34), crossed circles, 3170 Hz (Ref. 32), stars, 484 Hz (Ref. 32).

slightly smaller than the frequency of the maximum of the relaxation susceptibility (Fig. 6), while for silica it is slightly higher (Fig. 7). The rescaled data of Figs. 6 and 7 are plotted in Fig. 8. Indeed, in both cases a master curve is found for all temperatures. It shows an exponential distribution; assuming such an exponential high-energy tail of $g(V)$ we estimate a width of $V_0=570$ K for CKN and 319 K for silica, showing a good agreement with the temperature dependence of the exponent α, cf. Sec. III C. We note that the scaling shows one and the same V_0 for all temperatures, both for CKN and silica.

In the case of silica (where a lot of data, obtained by different experimental probes, exist) the value $\nu_0=800$ GHz (corresponding to $\tau_0=(2\pi\nu_0)^{-1}=0.2$ ps) within experimental errors agrees with those obtained by comparing the internal friction and dielectric loss at different frequencies,[30] or by evaluating the variation of the sound velocity at temperatures below some 15 K.[34]

Figure 9 shows a comparison of the distribution function $g(V)$ obtained from the light scattering (data from Fig. 8) with that obtained from internal friction for silica.[22] The value $\nu_0=800$ GHz is used for the rescaling of all the data sets. Since the amplitude of the light-scattering susceptibility is normalized to the internal friction at the frequency of the Brillouin lines (≈ 35 GHz),[28,22] the only parameter for the rescaling is ν_0, and this value is taken from the light-scattering experiment. Within the scatter of the different sets of experiments, a good agreement of the curves by the different methods is found. The biggest deviation of the acoustic data from the rescaled light scattering data is about a factor of 2, i.e., it is about the same than the deviations from different acoustic experiments. Within this precision we obtain a master curve for all the available data in the temperature range $10\,\mathrm{K}<T<200$ K. This means that within that precision all the experimental data can be described by two single parameters, $V_0=319$ K, and $\nu_0=800$ GHz over the frequency range $500\,\mathrm{Hz}\lesssim\nu\lesssim 500$ GHz. It further means that the power-law behavior approximately extends over the same range, as has been shown in Ref. 22. In principle, one experiment is sufficient to obtain the barrier distribution. The light-scattering experiment, however, probes the frequency and temperature dependence of the relaxational contribution simultaneously, enabling a cross-test of the model. In fact, it has already been shown that for several glasses such a rescaling does not lead to a master curve.[18,21]

It should be noted that regarding the parameter V_0 slightly different values have been reported in the literature.[27,34,35,40] This is partly due to the fact that some acoustic data appear more *flat* at low barrier heights in Fig. 9, and partly due to the fact that a different form of $g(V)$ has been used to describe the data. Only considering single sets of acoustic data, some works found that a Gaussian (or, indeed a modified Gaussian) describes the data better than an exponential.[27,30,34,35] However, the temperature and frequency dependence of the light-scattering data presented here cannot be described simultaneously by a temperature-independent distribution $g(V)$ of Gaussian shape. For CKN this is demonstrated in Figs. 6(b) and 10, see also Sec. IV C below; without proof, a similar result is obtained in the case of silica. On the present record of different sets of data, however, it is not possible to decide, whether the agreement could be improved by considering either a slight temperature dependence of $g(V)$ or small deviations of the purely exponential shape. The different sets of data for both silica and CKN can be reasonably well described by a temperature-independent distribution of barrier heights of exponential shape.

3. Numerical evaluation of relaxation spectra

In the preceding sections it was shown that within the ADWP model the data can be consistently described by assuming a flat distribution of asymmetry parameters, $f(\Delta)=f_0$, and an exponential distribution of barrier heights, $g(V)=V_0^{-1}\exp(-V/V_0)$. These findings can now be inserted in Eq. (6), and the double integral can be evaluated numerically. Figures 6(a) and 7 show the results of this integration

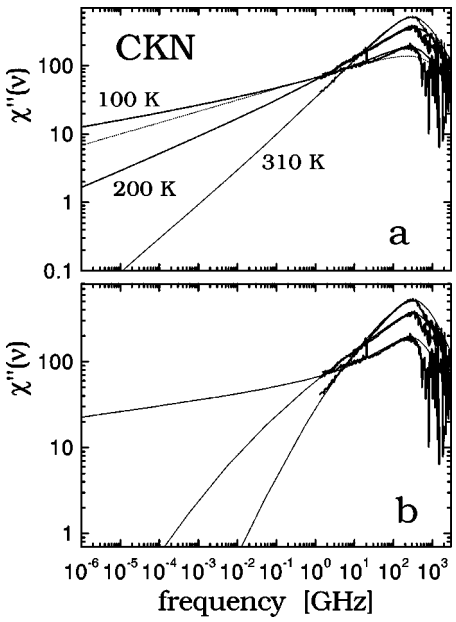

FIG. 10. (a) Low-frequency asymptotics of the calculated spectra: SPM–solid lines, ADWP model with exponential distribution of barrier heights–dotted line. (Same as Fig. 6) (b) Fit of the experimental relaxation spectra, $\chi''(\omega)$, for CKN by the generalized soft-potential model with a Gaussian cutoff of the distribution function of barrier heights, Eq. (35). The parameters of Eq. (35) are $b=0.6$, $V_0=1190$, 1330, and 3330 K for $T=310$, 200, and 100 K, respectively.

together with the experimental data. This constitutes an even more rigorous test of the model, since now no approximations are made and since also the temperature dependence of the amplitude of the spectra is given by the model (being constant over the entire temperature range). This procedure allows also a more accurate determination of the attempt frequency ν_0: ν_0 determines both the position of the maximum of the relaxation spectrum and the position, where spectra for different temperatures cross. While the first could be influenced by the validity of the substraction procedure, the latter occurs in a frequency range, where the substraction procedure has no discernible influence on the data (cf. Fig. 7). This procedure yields $\nu_0=222$ GHz for CKN and $\nu_0=800$ GHz for silica, in good agreement with the values obtained by the rescaling (cf. Sec. IV B 2).

At low frequencies there is a good agreement of the measured and calculated spectra. However, this model cannot fit the shape of the relaxation spectrum near the maximum. In Fig. 6(a) the fit of the relaxation spectrum at 300 K in CKN by the ADWP model, assuming an exponential $g(V)$ is shown. The width of the distribution $g(V) \propto \exp(-V/k_B \cdot 610\,\mathrm{K})$ is taken from the fit to the temperature dependence of α, cf. Fig. 4. Near the maximum of the relaxation spectra, there are deviations between calculations and experimental results: ν_0 appears to be lower than the position of the maximum of the experimental data, and the spectra predicted by the model are too broad compared to the measured ones near the maximum. Regading the position of the maximum, a good agreement is obtained, if one assumes a weak temperature dependence of the amplitude of the relaxations, i.e., assuming that the prefactor A in Eq. (10) increases by 20–30 % from 100 K to 310 K.

The exact shape of the spectrum depends on the details of the distribution of the relaxation times, or, in other words, on the details of $g(V)$. Here it appears that the ADWP model could be slightly modified in order to improve the agreement in the area of the maximum. In Sec. IV C below we will show results considering an enhancement of the barrier-distribution function at low barrier heights as it is predicted by the soft-potential model.

In fact, the actual relaxation spectra show an inrease compared to the calculated spectra at frequencies lower than the maximum of the relaxation spectrum for both systems investigated. (This remains true for CKN even if a larger ν_0 is used in order to obtain a better agreement near the maximum.) At frequencies above the maximum of the relaxation spectra the experimental data decrease more rapidly than the Debye behavior of the calculations. At present it is not possible to decide, if these deviations are due to the fact that the substraction procedure is not fully justified in that frequency range, or if small deviations of a purely exponential distribution $g(V)$ could lead to a better description of the data. The second explanation would imply a temperature dependence of the distribution function (see Sec. IV C below). It is interesting to note that the asymptotic power-law behavior extends to higher frequencies as would be expected according to the simple model.

Within the ADWP model the integral over the spectral density, S_r [Eq. (4)], does not depend on temperature; taking $\chi_r''(\nu)$ from Eq. (7) or Eq. (10) one obtains

$$S_r = \pi f_0 A. \tag{15}$$

As it was said in Sec. III, in CKN the integral over the relaxation spectrum δ_0^2 increases only by 20% when T increases by a factor of 3 from $T=100$ K up to room temperature. This is in a rough agreement with the ADWP model; 20% are about the accuracy of our extrapolations and subtractions procedures at low temperatures. On the other hand, it cannot be excluded that at least a part of this increase may be attributed, e.g., to a small increase of the density of defects that takes place even at temperatures below T_g or to a contribution of another fast-relaxation mechanism. In that case, one also obtains a better agreement concerning the high frequency cutoff ν_0 of CKN.

4. Correlation function of the fast relaxation in the time domain

The correlation function of the fluctuations of the polarizability tensor $F(t)$ can be evaluated as a Fourier transform of the spectral density $\chi_r''(\nu)/\nu$. Qualitatively, it is clear that the Debye behavior of the susceptibility at high frequencies corresponds to a simple exponential decay of the correlation function $F(t)$ at short times, $t \ll \tau_0$. On the other hand, the power-law behavior of $\chi_r''(\nu)$ at low frequencies should lead to a stretched behavior of the correlation function at $t \gg \tau_0$. Here we estimate $F(t)$ within the frame of the ADWP model in order to show that the fast relaxation itself may produce a transition from a Debye-like to a stretched behavior of the

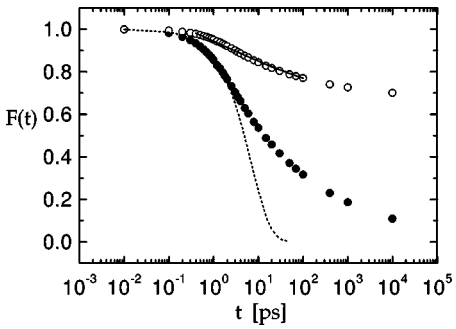

FIG. 11. Time-correlation function that corresponds to the ADWP susceptibility. Solid circles: time-correlation function $F(t)$, Eq. (19), with $\alpha=0.23$. A fit by a simple exponential is shown by the dotted line. Open circles: the same $F(t)$ superimposed on a constant background that corresponds to the Debye-Waller factor. For comparison a fit by a stretched exponential with $\beta=0.4$ is shown by the solid line.

time-correlation function normally ascribed to the primary α relaxation in supercooled liquids.[5] The correlation function can be expressed via the distribution function $G(\tau)$ of the relaxation times as follows:

$$F(t)=\int_0^\infty e^{-t/\tau}G(\tau)d\tau. \tag{16}$$

The exponential distribution of potential barriers (9) with the activation-temperature dependence of the relaxation times (8) gives

$$G(\tau)=\frac{\alpha\tau_0^\alpha}{\tau^{1+\alpha}} \quad \text{at} \quad \tau\geqslant\tau_0 \tag{17}$$

$$G(\tau)=0 \quad \text{at} \quad \tau<\tau_0. \tag{18}$$

With this $G(\tau)$ one has the following expression for the correlation function:

$$F(t)=\alpha\tau_0^\alpha\int_{\tau_0}^\infty e^{-t/\tau}\tau^{-\alpha-1}d\tau=\alpha(t\tau_0)^{-\alpha}\gamma(\alpha,t/\tau_0), \tag{19}$$

where

$$\gamma(\alpha,x)=\int_0^x e^{-z}z^{\alpha-1}dz \tag{20}$$

is the incomplete Γ function. The correlation function $F(t)$ given by Eq. (19) is shown in Fig. 11. It exhibits a behavior that can be interpolated in fair accuracy by a Debye function at $\tau<\tau_0$ and a stretched decay at longer times. In Fig. 11 both $F(t)$ and the same normalized function superimposed on some constant, which corresponds to the Debye-Waller factor, are shown. For comparison, we display a fit by a stretched exponent of the form $\exp[-(t/\tau_0)^\beta]$ that is normally used to fit the time-correlation functions in glass formers in the presence of the α relaxation.[5] However, in our case, deep in the glassy state, there are no effects of the α relaxation in the chosen time window. The behavior demonstrated by the correlation function in Fig. 11 (i.e., the transition from the Debye to a stretchedlike relaxation at the cross-over time ~ 1 ps) is an intrinsic property of the fast relaxation.

We note that the results regarding the transition from the stretched behavior to the Debye one is in agreement with that of neutron-scattering experiments on polymers,[5] where a Debye behavior was observed in the intermediate-scattering function $S(Q,t)$ at short times and a stretched behavior at longer times. The characteristic time at which $S(Q,t)$ changes its behavior from Debye to stretched exponential relaxation, $t_c\sim 1$ ps, was found to be rather temperature independent, in agreement with the data in Figs. 6 and 7, and has the same value by order of magnitude. However, in Ref. 5 spectra at $T>T_g$ were analyzed and the stretched part of the relaxation function was attributed to the high-frequency wing of the primary α relaxation. It is obvious that in our case the tail is related to the low-frequency wing of the fast-relaxation spectrum (cf. Fig. 6), at frequencies higher than the susceptibility minimum that separates α relaxation and fast dynamics in frequency domain. One may speculate whether in the case of the polymer PVC in Ref. 5 the dynamics revealed by neutron scattering are completely determined by fast dynamics that can be described within ADWP model.

C. Soft-potential model

The SPM Ref. 41 is a phenomenological model of dynamics in glasses. In particular, it makes detailed predictions on relaxations in ADWP's, on one-well potentials, as well as on soft vibrations, i.e., the so-called boson peak. Because of the importance of this model we discuss the predictions of SPM concerning the fast relaxation. We will show that although the standard SPM cannot correctly describe the spectral shape of the fast relaxation in silica and CKN, a natural generalization of the model's assumptions leads to a good agreement with our experimental data.

The SPM describes excitations in glasses that are localized within effective potentials in the form of fourth-order polynomials,

$$U(x)=\varepsilon_0[\,\eta(x/a)^2+\xi(x/a)^3+(x/a)^4]. \tag{21}$$

Here x is a generalized coordinate, a is the average-interatomic distance, ε_0 is a characteristic atomic energy of the order of a few 10 eV. The parameters η and ξ vary from site to site. The distribution function $F(\eta,\xi)$ of these parameters is the essential point of the model. It is assumed that this distribution is flat and proportional to the factor $|\eta|$ that accounts for the stability of the potential with respect to infinitesimal atomic displacements,

$$F(\eta,\xi)=|\eta|P_0, \tag{22}$$

where P_0 is a constant. With different values of parameters the fourth-order polynomial potential can describe, of course, all kinds of asymmetric double-well potentials, in particular, those which correspond to the tunneling systems. In some region of the parameters the polynomial (21) describes a single-well potential with a small force constant; within the SPM the respective excitations correspond to the boson peak. Of course, the SPM includes the ADWP model if one

chooses an appropriate distribution function $F(\eta,\xi)$, different from the standard one of Eq. (22). This point will be discussed in more detail below in this section.

Within the SPM the Raman-scattering intensity is determined by the inverse sound absorption length[41] $l^{-1}(\nu)$,

$$\frac{I(\nu)}{n(\nu)+1} \propto \chi''(\nu) \propto l^{-1}(\nu)/\nu. \tag{23}$$

In the frequency range 0.5–100 GHz and temperature range 20–310 K relevant to the experimental results of the present paper the main contribution to the susceptibility in SPM comes from thermally activated jumps in ADWP's.[52] In addition, the relaxation absorption by soft harmonic oscillations in the one-well potentials that arises due to the cubic anharmonic term in Eq. (21) also gives a contribution.[52] In the regime of thermally activated jumps the SPM predicts a weak logarithmic dependence of the light-scattering susceptibility on frequency[52]:

$$\chi_r''(\nu) \propto l_{DW}^{-1}/\nu = \frac{\pi C}{v}\left(\frac{T}{W}\right)^{3/4} [\ln(1/2\pi\nu\tau_0)]^{-1/4}, \tag{24}$$

where v is the sound velocity, C is a characteristic parameter of both SPM and tunneling model, $W=\varepsilon_0\eta_L^2 \sim 2-5$ K, $\eta_L = (\hbar^2/2Ma^2\varepsilon_0)^{1/3} \sim 10^{-2}$, M is the effective mass of the oscillator, a is a characteristic interatomic length and $\tau_0 \sim 10^{-12}-10^{-13}$ s is the attempt time, $2\pi\nu\tau_0 \ll 1$. This expression certainly cannot describe the power-law spectrum of the fast relaxation presented in Figs. 6 and 7.

The second mechanism, i.e., the relaxation absorption by the soft harmonic oscillations in the one-well potentials, l_{HO}^{-1}, gives contributions at temperatures $T \gg \nu$. This mechanism, in principle, should be relevant for our data. Three frequency ranges with different behavior of $l_{HO}^{-1}(\nu)$ can be separated for this mechanism.[52]

(i) The very low frequency region, $\nu \ll W(E_0/E_c)^2$, where $E_0 \approx 3W$ and $E_c = (2\pi\rho\hbar^3 v^5/\gamma^2)^{1/2}$, ρ is the density and γ is the deformation potential of the two-level systems. Typically, $W(E_0/E_c)^2$ is on the order of 10 GHz.[52] In this regime the SPM predicts a linear dependence of $\chi_r''(\nu)$ on frequency,

$$\chi_r''(\nu) \propto l_{HO}^{-1}/\nu = \frac{32\sqrt{2}CT}{27vE_0}\left(\frac{E_c}{E_0}\right)^2 \frac{\nu}{W}. \tag{25}$$

Our experimental data show no signs of a linear frequency dependence of the light-scattering susceptibility at any temperature, even at lowest frequencies ~ 1 GHz. Additionally, the amplitude of such a relaxation is small in comparison with that due to thermally activated jumps in ADWP.

(ii) At intermediate frequencies, $W(E_0/E_c)^2 \ll \nu \ll W(2T/E_c)^2$ (typically this is the region of the Brillouin lines) one has

$$\chi_r''(\nu) \propto l_{HO}^{-1}/\nu = \frac{16\pi CTW^{1/2}}{9vE_c}\nu^{-1/2}.$$

Such a behavior obviously does not correspond to our data.

(iii) Finally, at high frequencies, $\nu \gg W(2T/E_c)^2$, the relaxation of the soft harmonic oscillation in the SPM is described by the Debye-like law in qualitative agreement with the experiment,

$$\chi_r''(\nu) \propto l_{HO}^{-1}/\nu = \frac{32\pi^2 CT^2 W}{27vE_c^2}\nu^{-1}. \tag{26}$$

To summarize, the SPM in its standard form fails to describe the spectral shape of fast relaxation correctly; both mechanisms, thermally activated jumps in ADWP's and relaxation of soft harmonic oscillators, cannot describe the observed fast-relaxation susceptibility below the maximum.

However, the SPM predictions are obtained under the particular assumption on the distribution of the soft potential parameters η and ξ, Eq. (22). A generalization of this distribution in principle may improve the situation. We know from the previous section that the mechanism based on thermally activated jumps in ADWP's with an exponential distribution of barrier heights well describes the experimental spectrum of the fast relaxation (ADWP model[29]). On the other hand it is clear that any ADWP with a barrier height V and an asymmetry Δ can be represented by the effective fourth-order potential (21) with a specific choice of the parameters η and ξ. It is interesting to consider what kind of distribution of η and ξ would correspond to the exponential distribution of the barrier heights and a flat distribution of the asymmetry, i.e., to ADWP model. The SPM with such a distribution of η and ξ should well describe the experimental fast relaxation spectrum.

The connection between the parameters of an ADWP, namely V, Δ and that of the respective effective potential, η, ξ, is the following[41]:

$$V = \frac{W\eta^2}{4\eta_L^2} \tag{27}$$

and

$$\Delta = \frac{W|\xi|\eta^{3/2}}{\sqrt{2}\eta_L^2}. \tag{28}$$

The distribution function, Eq. (22), of the standard SPM in terms of V and Δ is described by the function $\Phi(V,\Delta)$,

$$\Phi(V,\Delta) = g_{SPM}(V) = \frac{P_0\eta_L^2}{W^{5/4}V^{3/4}}. \tag{29}$$

The Jacobian of the transformation from the parameters η, ξ to V, Δ is equal to $W^2\eta^{5/2}/2\sqrt{2}\eta_L^4$. Introducing an exponential decaying factor in the standard SPM distribution function (29) may be considered as a natural generalization of the model to improve agreement with respect to experimental results. So, we introduce a modified distribution function $\bar{g}_{SPM}(V)$,

$$\bar{g}_{SPM}(V) = \frac{fP_0\eta_L^2}{W^{5/4}V^{3/4}}\exp(-V/V_0), \tag{30}$$

where $f \sim 1$. In terms of the SPM parameters η and ξ the modified distribution function that corresponds to $\overline{g}_{\mathrm{SPM}}(V)$ has the Gaussian cutoff

$$F(\eta,\xi) = |\eta| P_0 \exp(-\eta^2/\eta_0^2), \tag{31}$$

where

$$\eta_0 = 2\eta_{\mathrm{L}} \sqrt{\frac{V_0}{W}}. \tag{32}$$

It is reasonable that the distribution of the force constants in a glass has a Gaussian cutoff. Since V_0 typically is on the order of $500-1000\,\mathrm{K}$ and $W \sim 3-5\,\mathrm{K}$ one has $\eta_0 \sim (20-40)\,\eta_{\mathrm{L}}$. This means that η_0 corresponds to typical force constants of the material and the Gaussian factor in Eq. (31) just describes the Gaussian high-frequency cutoff of the spectrum of acoustical vibrations of a disordered lattice. In particular, taking for silica the data from Ref. 52, $W = 3.3\,\mathrm{K}$, $\eta_{\mathrm{L}} = 2.3 \times 10^{-3}$, one obtains $\eta_0 = 22\,\eta_{\mathrm{L}} = 0.05$. The value of η_0 is unimportant as long as the SPM focuses on the tunneling properties of glasses. However, at higher temperatures the correct behavior of the distribution function at high values of η becomes important and, in fact, determines the spectral shape of the low-frequency wing of the fast-relaxation spectrum. In terms of the cutoff parameter η_0 the slope α of the low-frequency power-law wing is

$$\alpha = \frac{4T}{\varepsilon_0 \eta_0^2} \tag{33}$$

If $\eta_0 \to \infty$, i.e., $\exp(-\eta^2/\eta_0^2) = 1$, one has $\alpha \to 0$ and only the weak logarithmic dependence (24) of the low-frequency wing remains.

The factor $V^{-3/4}$ in the distribution function $\overline{g}_{\mathrm{SPM}}(V)$ enhances the contribution of the ADWP's with small barrier heights in the relaxation spectrum. As a result, the relaxation spectrum is modified at high frequencies, near the maximum, in comparison with the case of a purely exponential distribution function. In Fig. 6 we show the fit (dashed line) of the experimental data for CKN that was performed with the barrier-height distribution function of the type

$$g(V) = A V_0^{b-1} V^{-b} \exp(-V/V_0), \tag{34}$$

where A is a normalization constant on the order of one, by applying Eq. (7). In a log-log representation the low-frequency wing of the fitting function contains two parts with slightly different slopes [Fig. 10(a)] that exhibit a kind of *antiknee* spectrum. The *antiknee* is more pronounced at $T = 100$ K and is practically unobservable at 310 K. The asymptotic power-law behavior of the fit function begins at frequencies on the order of 1 GHz, slightly lower than the low-frequency limit of our experiment. At higher frequencies the fitting function exhibits a power law with a higher exponent; this part of the spectrum well fits the experimental data in the region of the maximum. The fit is better than in the case of the exponential $g(V)$ since the spectrum is narrower near the maximum than that of the purely exponential distribution. The best fit corresponds to $b = 0.45$, in a reasonable agreement with the distribution function of the SPM Eq. (30). However, contrary to the pure exponential case [shown in Fig. 6(a)], it is impossible to fit the data at different temperatures using a single parameter V_0; the best fit gives $V_0 = 600$, 910, and 1250 K for $T = 310$, 200 and 100 K, respectively. In addition, the amplitude of the relaxation spectrum increases with temperature stronger than it is predicted by the ADWP model with the barrier distribution function of the SPM, Eq. (34): at $T = 310\,\mathrm{K}$ the experimental amplitude is higher by the factors 1.24 and 1.35 than that at $T = 200$ and 100 K, respectively, compared to the prediction of the model.

For comparison, we also consider a Gaussian tail of the barrier-height distribution function of the SPM, as it was used earlier for a description of the sound absorption data[36,35]:

$$g_{\mathrm{G}}(V) = A_1 V_0^{b-1} V^{-b} \exp(-V^2/V_0^2). \tag{35}$$

In terms of the SPM such a distribution function corresponds to the decay of $F(\eta,\xi)$ at high η as $\exp(-\eta^4/\eta_0^4)$. The result of the fitting is shown in Fig. 10(b). The fit is quite good; the values of the best fit parameters are $b = 0.6$, $V_0 = 1190$, 1330, and 3330 K for $T = 310$, 200 and 100 K, respectively. Again, V_0 depends on temperature, and the experimental amplitude is higher by 20% at 310 K than expected from the model. The low-frequency tails of the fitting functions (Fig. 10) behave differently in comparison with the case of the distribution function Eq. (34), in particular, in the Gaussian case they do not exhibit an asymptotic power-law spectrum. However, the frequency range of our experimental data is still too narrow to clearly distinguish between the results predicted by the distribution function Eqs. (34) and (35).

Concluding this section, the SPM in its standard formulation with the distribution function (24) cannot correctly describe the low-frequency wing of the fast-relaxation spectra obtained in the present work. However, a generalization of the distribution function, Eq. (31), taking into account the existence of a high-frequency cutoff of the acoustical spectrum, leads to essentially the same results as the ADWP model. In particular it gives a correct description of the spectral shape of the fast relaxation in the regime of thermally activated transitions. While the SPM yields a better fit to the relaxation data at higher frequencies compared to the ADWP model with a purely exponential distribution function, it implies an additional temperature dependence of the distribution function.

D. Vibration-damping model

The vibration damping model of Gochiyaev *et al.*[14] is a phenomenological model that deals not with the nature of the fast relaxation in glasses itself but rather with the question how the fast relaxation, whatever its nature, leads to quasielastic scattering. Two contributions to quasielastic scattering in glasses due to fast-relaxation processes may be distinguished: a direct scattering of light on relaxators,[38] or an indirect scattering when light is scattered by vibrations and the relaxators influence the scattering process only via a coupling to vibrations.[14] There are several arguments in favor of

the second mechanism[15,40,42] that are based on the similarity of the properties of the quasielastic spectrum and the boson peak. However, both mechanisms predict a very similar spectral shape of the quasi-elastic spectrum,[14,15,40,42] so taking the presented results one cannot distinguish between the direct and indirect mechanisms of the quasielastic scattering.

Let us consider this point in more detail. Within the vibration-damping model, the intensity of the one-phonon light scattering by a harmonic excitation with a frequency Ω, $I_\Omega(\nu)$, is determined by the imaginary part of its response function $\chi(\nu,\Omega)$,

$$I_\Omega(\nu)\propto[n(\nu)+1][C(\Omega)/\Omega]\chi''_\Omega(\nu) \tag{36}$$

$$\chi_\Omega(\nu)=-[\nu^2-\Omega^2+M_\Omega(\nu)]^{-1}, \tag{37}$$

where $M_\Omega(\nu)=M'_\Omega(\nu)+iM''_\Omega(\nu)$ is a frequency-dependent damping term that has both real and imaginary parts and $C(\Omega)$ is the coupling constant of light to the vibration; the extra Ω in denominator of Eq. (36) is a standard factor that originates from the squared-matrix element of a harmonic oscillator. The damping term arises due to the interaction of the harmonic mode with other modes in the system, in particular, with relaxation modes. The imaginary part of the susceptibility that determines the light-scattering intensity is equal to

$$\chi''_\Omega(\nu)=\frac{M''_\Omega(\nu)}{[\nu^2-\Omega^2+M'_\Omega(\nu)]^2+[M''_\Omega(\nu)]^2}. \tag{38}$$

At low enough temperatures, when the damping is small $[M''_\Omega(\nu)\ll\Omega^2]$ (regarding boson peak vibrations and temperatures below T_g, see, e.g., Ref. 15) the susceptibility at low frequencies $\nu\ll\Omega$ can be separated from the vibrational spectrum; from Eq. (38) it follows that in this case $\chi''_\Omega(\nu)$ is determined only by the imaginary part of the damping term,

$$\chi''_\Omega(\nu)\approx M''_\Omega(\nu)/\Omega^4. \tag{39}$$

At these conditions the reduced quasielastic light-scattering intensity can be written in the form

$$\chi''(\nu)\propto\frac{I^{\mathrm{QES}}}{n(\nu)+1}=\int M''_\Omega(\nu)C(\Omega)g(\Omega)d\Omega/\Omega^5. \tag{40}$$

The last expression shows that the frequency dependence of the quasielastic light scattering is determined by $M''_\Omega(\nu)$ averaged over the vibrations in the region of the boson peak,[53] i.e., approximately can be described by $M''_\Omega(\nu)$ for Ω at the maximum of the boson peak Ω_b multiplied by a factor $D=\int C(\Omega)g(\Omega)d\Omega/\Omega^5$

$$\chi''(\nu)\propto DM''_{\Omega_b}(\nu). \tag{41}$$

The interaction of vibrations with relaxation modes can be described by a similar expression as in the case of the interaction of light with relaxations. E.g., relaxational motion may change the effective electric or elastic dipole giving rise to the damping of vibration or light wave, respectively.[29] This means that within the Gochiyaev model[14] the spectrum of the quasielastic light scattering may be very similar to the spectrum of direct scattering of light on the relaxation modes. In this sense, the analysis of the spectral shape of the fast relaxation performed in the present paper cannot decide the validity of the Gochiyaev model.[14] Note again that relaxational and vibrational contributions can be separated unambiguously within this model at small damping, in particular, in our case.

E. Anharmonic vibration model of fast relaxation

Recently it was shown that the cubic anharmonicity of vibrations may give a contribution to the quasielastic light scattering.[42] In the temperature range of the glass transition the amplitude of this contribution is in a good agreement with the experimental data on the quasielastic light scattering for a lot of glasses for which the respective data are available.[42] This means that the anharmonic vibration interaction may be a dominant source of fast relaxation at temperatures near T_g. The underlying relaxation process corresponds to fluctuations of the phonon density. For boson-peak vibrations the respective relaxation time is on the order of picoseconds. The strength of the fast relaxation—that is the ratio of the integrals of the quasielastic to the vibrational contribution—was found to be proportional to the squared Grüneisen parameter γ. In this theory, the intensity of the quasielastic light scattering due to the vibration anharmonicity can be expressed, like in the Gochiyaev model, cf. Eq. (40), with the following damping term,

$$M''_\Omega(\nu)\approx\frac{\nu\Omega^2T}{Mv^2}\int_0^{\Omega_m}\frac{\gamma^2(\Omega')\tau(\Omega')g(\Omega')d\Omega'}{1+\nu^2\tau^2(\Omega')}. \tag{42}$$

Here $\tau(\Omega')$ is the relaxation time of the phonon-density fluctuation, $g(\Omega')$ is the density of the vibrational states, M the molecular mass, v the sound velocity, and Ω_m a frequency near the end of the acoustic spectrum. Assuming for γ^2 some average value in the region of the boson peak, and a simple power-law frequency dependence for both the density of states and the relaxation time, $g(\Omega)=B_g\Omega^\sigma$ and $\tau^{-1}(\Omega)=B_\tau\Omega^{2\beta}$ one arrives at the spectrum of the fast relaxation

$$I_r^{\mathrm{QES}}(\nu)=S\nu^\alpha\int_{2\pi\nu\tau_0}^\infty\frac{x^{-\alpha}dx}{x^2+1} \tag{43}$$

($x=2\pi\nu\tau$) that has practically the same spectral shape as in the case of the ADWP model, Eq. (10) but with a different exponent,

$$\alpha=(\sigma+1)/2\beta. \tag{44}$$

The constant S is equal to

$$S=\frac{T\gamma^2B_g}{Mv^2B_\tau^{2-\alpha}}\int C(\Omega)g(\Omega)d\Omega/\Omega^4 \tag{45}$$

and $\tau_0=\tau(\Omega_m)$. The low-frequency tail of the spectrum $(2\pi\nu\tau_0\ll1)$ is described by a power law,

$$\chi''(\nu) \propto I_r^{\mathrm{QES}}(\nu) \approx \nu^{\alpha} \frac{\pi S}{2\cos(\pi\alpha/2)}, \tag{46}$$

while the high-frequency wing is the Debye-like,

$$\chi''(\nu) \propto I_r^{QES}(\nu) \approx (2\pi\nu\tau_0)^{-1} \frac{S}{(\alpha+1)\tau_0^{\alpha}}. \tag{47}$$

The exponent α defined by Eq. (44) is essentially temperature independent; the lack of knowledge on the frequency dependence of the relaxation time of the phonon-density fluctuations makes it impossible to predict α reliably. However, an estimate[42] shows that $\alpha = 0.3-1$. Within this theory, the relaxation-strength parameter δ_0^2 defined by Eq. (5) increases with temperature

$$\delta_0^2 = \gamma^2 \frac{T}{Mv^2}, \tag{48}$$

so the contribution of this mechanism is weak at low temperatures and stronger around the glass transition temperature. This is in contrast with the relaxation caused by thermally activated jumps in the ADWP's where the integral on the relaxation spectrum is temperature independent.

Both mechanisms, thermal activation in ADWP's and anharmonicity, may give a contribution to the fast-relaxation spectrum in glasses. Their relative intensity may be different in different substances and even at different temperatures in the same substance. Which mechanism dominates mainly depends on temperature and the ratio between the density of the ADWP and the Grüneisen parameter (see Ref. 21). As it was shown,[42] at T_g the contribution of the anharmonic mechanism is large enough to explain the amplitude of the fast relaxation for many materials for which data are available, in particular, for polymers like polystyrene and polycarbonate, for boron oxide, silica, glycerol, and some other glasses. However, the experimental results of the present paper can be correctly described, assuming that deep in the glassy state the ADWP mechanism is dominant both in CKN and silica.

V. CONCLUSION

Inelastic light-scattering spectra of two inorganic glass formers, CKN and silica, were measured in the spectral range 1 GHz–10 THz at temperatures well below T_g, $T = 19-310$ K. The fast relaxation spectra in these glasses show a power-law wing at low frequencies, exhibiting an exponent less than 1. In both CKN and silica this exponent is proportional to temperature. A deviation from the linear dependence is observed in silica at room temperature, where the value of the exponent becomes close to 1. The relaxational part of the susceptibility spectra in CKN has a maximum at a frequency $\nu_0 = 300$ GHz that does not show any appreciable temperature dependence; this corresponds to a cutoff of the relaxation-time distribution function at some minimum value τ_0 on the order of picoseconds. For silica, the observed value of $\nu_0 = 800$ GHz corresponds to $\tau_0 = 0.2$ ps.

We compare the experimental results with the predictions of existing models of fast relaxation. The data can be well described by a model considering thermally activated jumps in double well potentials.[29,37,38] We extract the distribution function of barrier heights from our light-scattering data; it shows an exponential shape. A comparison of the distribution function obtained from light scattering and internal friction yields, that the relaxational behavior of silica can be described by two parameters, namely $V_0 = 319$ K and $\nu_0 = 800$ GHz, over the frequency range $500\,\mathrm{Hz} < \nu < 800\,\mathrm{GHz}$ and for temperatures above some 10 K.

The soft-potential model can also describe the data well in the regime of thermally activated relaxation in the double-well potentials, provided that an upper cutoff value of the distribution function of the soft potential harmonic strength parameter is introduced. Considering the existing experimental evidence, it cannot be decided if slightly different assumptions about $g(V)$ could lead to a better description of the data. We would like to stress that the model of thermally activated relaxations in its simple form presented here cannot describe the spectra of the fast relaxation correctly for all glasses. As it was shown in Refs. 18 and 21, in some polymers and boron oxide the exponent α exhibits a temperature dependence different from the predictions of the models. This could be related with different mechanisms dominating the fast relaxation in different materials.

ACKNOWLEDGMENTS

We appreciate valuable discussions with H. Z. Cummins and support from J. Wuttke, L. Kador, J. R. Sandercock, and S. J. Zilker. This work has been supported by Deutsche Forschungsgemeinschaft through Sonderforschungsbereich 279. Furthermore, support by INTAS Grant No. 93-2185ext is gratefully acknowledged. A.P.S. thanks the Research Office of UA for financial support (Grant No. FRG1446).

*Present address: Physikdepartment E13, TU München, 85747 Garching, Germany. Email address: jowi@ph.tum.de

†On leave from Institute of Automation & Electrometry, Russian Academy of Sciences, Novosibirsk 630090, Russia.

[1] W. Götze and L. Sjögren, Rep. Prog. Phys. **55**, 241 (1992).

[2] B. Frick and D. Richter, Science **267**, 1939 (1995).

[3] J. Wuttke, W. Petry, G. Coddens, and F. Fujara, Phys. Rev. E **52**, 4026 (1995); B. Frick, B. Farago, and D. Richter, Phys. Rev. Lett. **64**, 2921 (1990); R. Zorn, A. Arbe, J. Colmenero, B. Frick, D. Richter, and U. Buchenau, Phys. Rev. E **52**, 781 (1995); A. Brodin, L. Börjesson, D. Engberg, L.M. Torell, and A.P. Sokolov, Phys. Rev. B **53**, 11 511 (1996); A. Mermet, N.V. Surovtsev, E. Duval, J.F. Jal, J. Dupuy-Philon, and A.J. Dianoux, Europhys. Lett. **36**, 277 (1996).

[4] U. Buchenau, C. Schönfeld, D. Richter, T. Kanaya, K. Kaji, and R. Wehrmann, Phys. Rev. Lett. **73**, 2344 (1994).

[5] J. Colmenero, A. Arbe, and A. Algeria, J. Non-Cryst. Solids **172-174**, 126 (1994).

[6] J. Wuttke, M. Seidl, G. Hinze, A. Tölle, W. Petry, and G. Coddens, Eur. Phys. J. B **1**, 169 (1998).
[7] G. Winterling, Phys. Rev. B **12**, 2432 (1975).
[8] R. Nemanich, Phys. Rev. B **16**, 1655 (1977).
[9] G. Carini, G. D'Angelo, G. Tripodo, A. Fontana, A. Leonardi, G.A. Saunders, and A. Brodin, Phys. Rev. B **52**, 9342 (1995).
[10] F. Terki, C. Levelut, J.L. Prat, M. Boissier, and J. Pelous, J. Phys.: Condens. Matter **9**, 3955 (1997).
[11] G. Li, W.M. Du, X.K. Chen, H.Z. Cummins, and N.J. Tao, Phys. Rev. A **45**, 3867 (1992).
[12] H.Z. Cummins, G. Li, W.M. Du, and J. Hernandez, Physica A **204**, 169 (1994).
[13] R.M. Pick, A. Aouadi, C. Dreyfus, R. Torre and P. Bartolini, J. Phys.: Condens. Matter **8**, 9593 (1996).
[14] V.Z. Gochiyaev, V.K. Malinovsky, V.N. Novikov, and A.P. Sokolov, Philos. Mag. B **63**, 777 (1991).
[15] V.N. Novikov, A.P. Sokolov, B. Strube, N.V. Surovtsev, E. Duval, and A. Mermet, J. Chem. Phys. **107**, 1057 (1997).
[16] V.N. Novikov, N.V. Surovtsev, E. Duval, and A. Mermet, Europhys. Lett. **40**, 165 (1997).
[17] A. Aouadi, M.J. Lebon, C. Dreyfus, B. Strube, W. Steffen, A. Patkowski, and R.M. Pick, J. Phys.: Condens. Matter **9**, 3803 (1997).
[18] N.V. Surovtsev, J. Wiedersich, V.N. Novikov, A.P. Sokolov, and E. Rössler, Phys. Rev. B **58**, 14 888 (1998).
[19] J. Gapińsky, W. Steffen, A. Patkowski, A.P. Sokolov, A. Kisliuk, U. Buchenau, M. Russina, F. Mezei, and H. Schober, J. Chem. Phys. **110**, 2312 (1999).
[20] H.C. Barshilia, G. Li, G.Q. Shen, and H.Z. Cummins, Phys. Rev. E **59**, 5625 (1999).
[21] N.V. Surovtsev, J.A.H. Wiedersich, E. Duval, V.N. Novikov, E. Rössler, and A.P. Sokolov, J. Chem. Phys. **112**, 2319 (2000).
[22] J. Wiedersich, S. Adichtchev, and E. Rössler, Phys. Rev. Lett. **84**, 2718 (2000).
[23] P. Lunkenheimer, A. Pimenov, and A. Loidl, Phys. Rev. Lett. **78**, 2995 (1997).
[24] M.E. Fine, H. van Duyne, and Nancy T. Kenney, J. Appl. Phys. **25**, 402 (1954).
[25] O.L. Anderson and H.E. Bömmel, J. Am. Ceram. Soc. **38**, 125 (1955).
[26] C.K. Jones, P.G. Klemens, and J.A. Rayne, Phys. Lett. **8**, 31 (1964).
[27] S. Hunklinger, in *Ultrasonics Symposium Proceedings*, edited by J. de Klerk (IEEE, New York 1974), pp. 493–501.
[28] R. Vacher, J. Pelous, F. Plicque, and A. Zarembowitch, J. Non-Cryst. Solids **45**, 397 (1981).
[29] K.S. Gilroy and W.A. Phillips, Philos. Mag. B **43**, 735 (1981).
[30] S. Hunklinger and M. v. Schickfus, in *Amorphous Solids: Low-Temperature Properties*, edited by W.A. Phillips, (Springer, Berlin, 1981), pp. 81–106.
[31] U. Bartell and S. Hunklinger, J. Phys. Colloq., **43**, C9489 (1982).
[32] A.K. Raychaudhuri and S. Hunklinger, Z. Phys. B: Condens. Matter **57**, 113 (1984).
[33] D.G. Cahill and J.E. Van Cleve, Rev. Sci. Instrum. **60**, 2706 (1989).
[34] D. Tielbürger, R. Merz, R. Ehrenfels, and S. Hunklinger, Phys. Rev. B **45**, 2750 (1992).
[35] R. Keil, G. Kasper, and S. Hunklinger, J. Non-Cryst. Solids **164-166**, 1183 (1993).
[36] K.A. Topp and D.G. Cahill, Z. Phys. B: Condens. Matter **101**, 235 (1996).
[37] N. Theodorakopoulos and J. Jäckle, Phys. Rev. B **14**, 2637 (1976).
[38] J. Jäckle, in *Amorphous Solids: Low-Temperature Properties*, edited by W. A. Phillips (Springer, Berlin, 1981).
[39] P.W. Anderson, B.I. Halperin, and C.M. Varma, Philos. Mag. **25**, 1 (1972); W.A. Phillips, J. Low Temp. Phys. **7**, 351 (1972).
[40] A.P. Sokolov, V.N. Novikov, and B. Strube, Europhys. Lett. **38**, 49 (1997).
[41] Yu.M. Galperin, V.G. Karpov, and V.I. Kozub, Adv. Phys. **38**, 77 (1989).
[42] V.N. Novikov, Phys. Rev. B **55**, R14 685 (1997).
[43] A.P. Sokolov, E. Rössler, A. Kisliuk, and D. Quitmann, Phys. Rev. Lett. **71**, 2062 (1993).
[44] N.V. Surovtsev, E. Duval, A. Mermet, and V.N. Novikov, J. Phys.: Condens. Matter **7**, 8077 (1995).
[45] J.R. Sandercock, Top. Appl. Phys. **51**, 173 (1982); S.M. Lindsay, M.W. Anderson, and J.R. Sandercock, Rev. Sci. Instrum. **52**, 1478 (1981); J.R. Sandercock, *Operator Manual for Tandem Interferometer* (unpublished).
[46] J. Wiedersich, Ph.D thesis, Universität Bayreuth, 2000.
[47] R. Shuker and R.W. Gammon, Phys. Rev. Lett. **25**, 222 (1970).
[48] A.J. Martin and W. Brenig, Phys. Status Solidi B **64**, 163 (1974).
[49] J. Wiedersich, N.V. Surovtsev, and N. Bagdassarov (unpublished).
[50] V.N. Novikov, Phys. Rev. B **58**, 8367 (1998).
[51] C.J.F. Böttcher and P. Bordewijk, *Theory of Electric Polarization* (Elsevier, Amsterdam, 1978), Vol. 2.
[52] V.L. Gurevich, D.A. Parshin, J. Pelous, and H.R. Schober, Phys. Rev. B **48**, 16 318 (1994).
[53] A.P. Sokolov, U. Buchenau, W. Steffen, B. Frick, and A. Wischnewski, Phys. Rev. B **52**, R9815 (1995).
[54] A. Fontana, D. Dell'Anna, M. Montagna, F. Rossi, G. Villiani, G. Ruocco, M. Sampoli, U. Buchenau, and A. Wischnewski, Europhys. Lett. **47**, 56 (1999).